NASA TECHNICAL NOTE

NASA TN D-8087

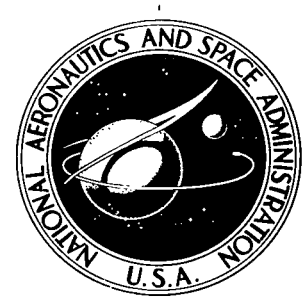

NASA TN D-8087

EFFECT OF STARVATION ON FILM THICKNESS AND TRACTION UNDER ELASTOHYDRODYNAMIC ROLLING AND SLIDING CONDITIONS

Lavern D. Wedeven

Lewis Research Center
Cleveland, Ohio 44135

NATIONAL AERONAUTICS AND SPACE ADMINISTRATION • WASHINGTON, D. C. • OCTOBER 1975

1. Report No. NASA TN D-8087	2. Government Accession No.	3. Recipie.

4. Title and Subtitle EFFECT OF STARVATION ON FILM THICKNESS AND TRACTION UNDER ELASTOHYDRODYNAMIC ROLLING AND SLIDING CONDITIONS	5. Report Date October 1975
	6. Performing Organization Code
7. Author(s) Lavern D. Wedeven	8. Performing Organization Report No. E-8412
9. Performing Organization Name and Address Lewis Research Center National Aeronautics and Space Administration Cleveland, Ohio 44135	10. Work Unit No. 505-04
	11. Contract or Grant No.
12. Sponsoring Agency Name and Address National Aeronautics and Space Administration Washington, D.C. 20546	13. Type of Report and Period Covered Technical Note
	14. Sponsoring Agency Code

15. Supplementary Notes

16. Abstract

Traction measurements under starved elastohydrodynamic conditions have been obtained for a point-contact geometry. Simultaneous measurements of the film thickness and the location of the inlet lubricant boundary were made. Optical interferometry was used to measure film thickness. The thickness of a starved film for combined rolling and sliding conditions varies with the location of the inlet boundary in the same way as previously found for pure rolling conditions. When the fluid velocity distribution is calculated in the inlet region by a Reynolds lubrication analysis, backflow is seen to occur over a portion of the inlet region. Backflow is essential for the establishment of a flooded condition. The location of certain fluid velocity conditions within the inlet region, as suggested in the literature, does not adequately describe the onset of starvation. For the same slide-roll ratio a starved film was observed to possess greater traction than a flooded film. Traction measurements under starved conditions were also compared with those under flooded conditions for equivalent shear rates in the Hertzian region. When the shear rates within the Hertzian region were low and the film was severely starved, the measured tractions were lower than expected. This may be due to large shear stresses developed by the large pressure gradients that are generated in the inlet region when it is severely starved.

17. Key Words (Suggested by Author(s))	18. Distribution Statement
Lubrication Elastohydrodynamics Bearings Traction Starvation	Unclassified - unlimited STAR Category 37 (rev.)

19. Security Classif. (of this report)	20. Security Classif. (of this page)	21. No. of Pages	22. Price*
Unclassified	Unclassified	39	$3.75

* For sale by the National Technical Information Service, Springfield, Virginia 22161

EEFECT OF STARVATION ON FILM THICKNESS AND TRACTION UNDER ELASTOHYDRODYNAMIC ROLLING AND SLIDING CONDITIONS

by Lavern D. Wedeven
Lewis Research Center

SUMMARY

Traction and film thickness measurements under starved elastohydrodynamic rolling and sliding conditions have been made for a point-contact geometry. Film thickness measurements were made optically by interferometry. Under combined rolling and sliding conditions, film thickness varies with the location of the inlet lubricant boundary in the same way as it does under pure rolling conditions.

The inlet fluid velocity distribution was estimated within an elemental strip along the centerline in the direction of rolling. Backflow occurs over a portion of the inlet region, which is essential for the establishment of a flooded condition. Certain fluid velocity conditions do not adequately define the location of pressure commencement or the onset of starvation.

In all cases tested, a starved film was observed to possess greater traction than a flooded film for the same slide-roll ratio. For a given slide-roll ratio, starving the film simply increased the shear rate in the Hertzian region. The shear rate depends on the degree of starvation. Measured shear rates increased an order of magnitude, from 40×10^4 seconds^{-1} to 400×10^4 seconds^{-1}, when the film was severely starved.

The relative increase in traction due to starvation for a given slide-roll ratio depends primarily on the thermal and fluid rheological conditions within the Hertzian region. The interaction of traction and starvation under the elastohydrodynamic (EHD) conditions tested appears too complicated to normalize the traction under a starved condition with its corresponding flooded value at the same slide-roll ratio. Thus, the traction measurements were considered in terms of the shear rate within the Hertzian region. In this way the flooded and starved traction measurements could be compared under conditions of similar heat generation. Except for low rates of shear, the measured tractions under starved conditions were found to be greater than the traction values under flooded conditions for the same shear rate. This can be explained by the improved heat conduction when the film is thinner (or starved).

When the shear rates in the Hertzian region were low and the film was severely starved, the measured tractions were much lower than expected. It is tentatively suggested that this may be due to the large shear stresses developed by the large pressure gradients that are generated in the inlet region when it is severely starved. Thus, the shear history of the fluid in the inlet region may affect the the traction developed in the Hertzian region.

INTRODUCTION

In the lubrication of bearings and gears the lubricant frequently functions as a coolant as well as a lubricant. These two functions are interrelated in that a fluid which is inherently a good lubricant may be required to provide less cooling. The amount of fluid required for cooling is usually very much greater than that required for lubrication. However, excess cooling fluid in confined spaces between rotating parts generates heat through churning and contributes to power consumption. These churning losses can be quite significant in high-speed bearings and gears.

In order to reduce churning losses, the design trend is to separate the lubrication and cooling flows. For example, advanced designs of high-speed turbine bearings use underrace cooling and provide small amounts of fluid between split inner raceways for lubrication (ref. 1). Gears are frequently cooled by supplying fluid to the demesh side of the gears (ref. 2). The heat generated in the conjunction zone between the gear teeth is conducted into the oil, which is then flung off the gear teeth before they mesh again. The residual oil remaining on the gear teeth prior to meshing should be small enough to avoid significant churning losses in the gear mesh but large enough to provide adequate lubrication.

For high-speed applications, mist lubrication of bearings and gears is frequently used. Here lubrication is achieved by a very small quantity of fluid in the form of a mist, and cooling is achieved from the gas phase of the mist.

Clearly, there is a definite trend in high-speed bearings and gears to limit the supply of fluid for the purpose of lubrication so that power consumption and heat generation can be reduced. In addition, it has been standard practice in the field of gyroscope bearings to supply only minute quantities of fluid in order to achieve very low and constant torque for optimum performance. Furthermore, the conjunction regions of many bearings and gears may be fed with a limited lubricant supply, not by design but by accident. The critical areas of lubrication are usually in confined spaces where lubricant supply is difficult to penetrate, and high rotative speed causes the lubricant to be expelled from the system.

Thus, it is important to understand the influence of a restricted or starved lubricant supply and distribution on lubrication. The influence of starvation on film thickness has been shown theoretically for conditions of point contact (ref. 3) and line contact (refs. 4 to 6). These solutions have been verified experimentally under rolling conditions (refs. 3 and 7). The present study was conducted to investigate the influence of lubricant supply on traction, as well as on film thickness, for various degrees of rolling and sliding. There have been occasional references to the important effect of starvation on traction between surfaces in relative sliding (refs. 8 and 9). But no thorough investigation has been performed under the conditions of elastohydrodynamic lubrication found in gears and rolling-element bearings.

In this investigation, traction between a ball and transparent disk was measured for various quantities of lubricant. Optical interferometry was used to measure oil film thickness. The interference fringes were recorded by high-speed photography, which also serves as a means for obtaining the quantity of lubricant.

SYMBOLS

a	Hertzian radius, m (in.)
E_1, E_2	modulus of elasticity of ball and transparent disk materials, N/m^2 (psi)
E'	reduced elastic modulus, $\frac{1}{E'} = \frac{1}{2}\left(\frac{1 - \sigma_1^2}{E_1} + \frac{1 - \sigma_2^2}{E_2}\right)$, N/m^2 (psi)
h	film thickness, μm (μin.)
h_b	film thickness at inlet lubricant boundary, μm (μin.)
h_0	film thickness at center of the Hertzian region, μm (μin.)
$(h_0)_f$	central film thickness under flooded conditions, μm (μin.)
h/h_0	dimensionless gap thickness
h_b/h_0	dimensionless gap thickness at inlet lubricant boundary
$h_0/(h_0)_f$	ratio of starved to flooded film thickness
h_r	film thickness at rear constriction, μm (μin.)
h_s	film thickness at side constrictions, μm (μin.)
k	thermal conductivity, W/(m)(k) (cal/(sec)(cm)(^oC))
p	pressure, N/m^2 (psi)
q	reduced pressure, $(1/\alpha)(1 - e^{-\alpha p})$, N/m^2 (psi)
q_v	heat generation, $J/(m^3)$(sec) (cal/(cm^3)(sec))
R	reduced radius of curvature, $\frac{1}{R} = \frac{1}{R_1} + \frac{1}{R_2}$, cm (in.)
R_1, R_2	radius of contacting bodies of ball and disk, cm (in.)
S	inlet distance measured from inlet lubricant boundary to leading edge of Hertzian region, cm (in.)
S_f	inlet distance necessary to obtain a flooded film thickness, cm (in.)

S/S_f	starvation parameter, $\dfrac{Sa^{1/3}}{3.52\left[R(h_0)_f\right]^{2/3}}$
t_0	time of transit through one-half of Hertzian region, $a/\bar{u}$, sec
u_1	surface velocity of ball, cm/sec (in./sec)
u_2	surface velocity of disk, cm/sec (in./sec)
$\bar{u}$	rolling velocity, $(u_1 + u_2)/2$, cm/sec (in./sec)
$\dfrac{u_1 - u_2}{\frac{1}{2}(u_1 + u_2)}$	slide-roll ratio
x, y, z	coordinates, m (in.)
α	pressure-viscosity coefficient, $(N/m^2)^{-1}$ $((psi)^{-1})$
σ_1, σ_2	Poisson's ratio of ball and disk materials
Λ	$\dfrac{kt_0}{h_0^2}$
μ	local viscosity of lubricant, N-sec/m^2 (lbf-sec/ft^2)
μ_0	ambient viscosity of lubricant, N-sec/m^2 (lbf-sec/ft^2)

BASIC CONCEPTS AND EQUATIONS

The influence of starvation on elastohydrodynamic lubrication deals with the supply and distribution of lubrication in the vicinity of the conjunction region and how this supply influences the hydrodynamic pressure generation between the surfaces. The hydrodynamic pressure generation between surfaces in motion is described by the Reynolds equation

$$\frac{\partial}{\partial x}\left(\frac{h^3}{\mu}\frac{\partial p}{\partial x}\right) + \frac{\partial}{\partial y}\left(\frac{h^3}{\mu}\frac{\partial p}{\partial y}\right) = 12\bar{u}\frac{\partial h}{\partial x} \tag{1}$$

where the rolling velocity $\bar{u}$ is one-half the sum of the surface velocities in the x-direction and p is the pressure generated in a film of thickness h having a viscosity μ. The assumptions involved in the Reynolds equation are given, for example, by Cameron (ref. 10).

If the side-leakage term is neglected, equation (1) can be integrated with respect to x to give

$$\frac{dp}{dx} = 12\bar{u}\,\mu\left(\frac{h - h_0}{h^3}\right) \tag{2}$$

where h_0 is the local film thickness at maximum pressure (where $dp/dx = 0$).

If the variation of viscosity with pressure is defined by the Barus equation (ref. 11)

$$\mu = \mu_0 e^{\alpha p} \tag{3}$$

then

$$e^{-\alpha p}\frac{dp}{dx} = 12\bar{u}\,\mu_0\left(\frac{h - h_0}{h^3}\right) \tag{4}$$

As explained by Dowson and Higginson (ref. 12), if the right side of equation (2) represents the pressure gradient of a variable-viscosity fluid, then the right side of equation (4) represents the pressure gradient of a constant-viscosity fluid. If the pressure generated by a constant-viscosity fluid is called the reduced pressure q, then

$$\frac{dq}{dx} = 12\bar{u}\,\mu_0\left(\frac{h - h_0}{h^3}\right) \tag{5}$$

and

$$\frac{dq}{dx} = e^{-\alpha p}\frac{dp}{dx} \tag{6}$$

Equation (5) is the integrated form of the Reynolds equation in terms of the reduced pressure, and equation (6) can be integrated to give the reduced pressure in terms of the actual pressure p and the pressure-viscosity coefficient α:

$$q = \frac{1}{\alpha}(1 - e^{-\alpha p}) \tag{7}$$

The influence of starvation can best be understood by considering certain predominant features and regions of elastohydrodynamic lubrication. A characteristic feature of elastohydrodynamic lubrication is that the elastic deformation and pressure distribution are very similar to the Hertzian condition of static contact. The Hertzian condition of static contact is illustrated in figure 1, and a typical elastohydrodynamic pressure and

shape are shown in figure 2. This near Hertzian condition of contact allows the conjunction region to be divided into three smaller regions, as shown in figure 2. Thus, a fluid particle that passes through the conjunction region will first of all encounter a converging inlet region followed by a parallel Hertzian region and finally a diverging outlet region.

Inlet Region

The converging geometry of the inlet region plays an important role in lubrication because the pressure generated hydrodynamically in this region determines the film thickness further downstream. The importance of the inlet region can be illustrated by considering the geometry term, $(h - h_0)/h^3$, in the integrated form of the Reynolds equation for the reduced pressure q, as given in equation (5). For a constant-viscosity fluid the reduced pressure gradient is a direct function of the value of the geometry term. The value of this term is plotted in figure 3 as a function of h/h_0, which is the dimensionless gap thickness in the inlet region. The contact geometry is assumed to be Hertzian with a parallel film of thickness h_0 in the Hertzian region. Thus, the value of the geometry term is zero in the Hertzian region, and significant values are obtained only in the inlet region. The geometry term reaches a maximum at $h/h_0 = 1.5$ and diminishes in the upstream direction as h/h_0 increases, reaching a small value at $h/h_0 = 9$. Since the geometry term is related to the rate of pressure generation (dq/dx), the curve of figure 3 represents the contribution of the geometry of the surfaces to the generation of hydrodynamic pressure.

Under typical elastohydrodynamic conditions the enhancement of viscosity with pressure also contributes to pressure generation in the inlet region. This is illustrated by the typical pressure and reduced-pressure curves shown in figure 4. The reduced pressure varies with the actual pressure according to equation (7). At low pressure, where h/h_0 is large, the actual pressure and reduced pressure are very similar. As the leading edge of the Hertzian region is approached the enhancement of viscosity with pressure becomes very pronounced. This causes the actual pressure to rise very rapidly while the reduced pressure, according to equation (7), approaches a limiting value of $1/\alpha$.

Inlet pressure, as shown in figure 4, plays an important role in lubrication. This hydrodynamic pressure can be thought of as a pressure which overcomes the Hertzian pressure at the leading edge of the Hertzian region so that fluid can become wedged between the surfaces.

Hertzian Region

The Hertzian region is dominated by the Hertzian pressure. This is the pressure that would exist if the surfaces were not separated by a lubricant film. The actual pressure differs from the Hertzian pressure only at the leading and trailing edges of the Hertzian region. Because the lubricant encounters very high pressures in the Hertzian region, its viscosity increases several orders of magnitude. This, along with the very thin parallel film in the Hertzian region, is the major cause of friction or traction between the bearing surfaces when they are in relative sliding.

Exit Region

The exit region exposes the fluid to a rapidly diverging geometry, which produces a negative pressure gradient and eventually subambient pressures. Since most fluids degas or cavitate under relatively low tensile stresses, this subambient hydrodynamic pressure is almost immediately terminated.

In brief, each of these three regions performs a particular function. The inlet region "pumps the film up," the Hertzian region "rides it," and the exit region "discharges it." It is convenient to consider the influence of starvation on film thickness and traction in terms of these regions.

EXPERIMENTAL APPARATUS AND PROCEDURE

Ball and Disk Materials

The optical elastohydrodynamic apparatus is shown in figure 5. It consisted basically of a ball which rode against a flat transparent disk (fig. 6). The disk rotated freely in an air bearing. The experimental balls were 2.063 centimeters (0.8125 in.) in diameter. The transparent disks were 10.2 centimeters (4 in.) in diameter. In order to obtain a range of maximum Hertzian pressure, both steel and tungsten carbide were used as ball materials and both quartz and sapphire were used as disk materials. Their mechanical properties are shown in table I, and their reduced elastic modulus E', defined as

$$\frac{1}{E'} = \frac{1}{2}\left(\frac{1 - \sigma_1^2}{E_1} + \frac{1 - \sigma_2^2}{E_2}\right) \tag{8}$$

is shown in figure 7. The various material combinations gave a range of E' from 1.1×10^{11} N/m^2 (15.9×10^6 psi) for quartz/steel to 6.38×10^{11} N/m^2 (92.5×10^6 psi) for sapphire/tungsten carbide.

Lubricant Supply

The ball was supported by three bearings, as shown in figure 6. The three bearings were contained within a lubricant reservoir. The spaces around the bearings were filled with the test lubricant. When the reservoir was completely filled, the ball was partially submerged in the test lubricant. The required lubricant supply for the starvation tests was achieved by limiting the lubricant supply in the reservoir. The motion of the support bearings within the reservoir very conveniently carried the test lubricant to the test-ball surface adjacent to the track on the ball. This method resulted in a uniform and steady inlet meniscus. An air cylinder below the lubricant reservoir provided the required test load on the ball.

Drive Mechanism and Speed Control

The ball was driven by a 0.15-kilowatt (1/5-hp) electric motor through a gearbox which had the ratios 1:1, 10:1, and 100:1. The motor was a variable-speed motor-generator with a very stable transistorized closed-loop control system. Speed regulation was much better than 1 percent.

Measurement of ball speed was achieved with a magnetic transducer in close proximity to a 100-tooth gear wheel attached to the motor shaft. The motor speed was displayed on a digital counter.

Torque Control and Disk Speed Measurement

A controlled braking torque was applied to the rotating transparent disk with a dynamometer which uses a hysteresis brake. The unique feature of the hysteresis brake is that it provides a constant torque independent of shaft speed. In order to obtain accurate slip measurements between the ball and the disk, it is important that the disk speed be measured accurately. This was achieved by using an optical transducer in conjunction with a 600-element encoder disk. Because of the large number of elements on a disk of 7.6 centimeters (3 in.) in diameter, it was necessary to pass the light from the light source through a 0.0172-centimeter (0.007-in.) slot so that only one shadow from the

encoder disk would fall on the photoelectric cell at a time. The disk speed was displayed on a digital counter and also recorded on a four-pen recorder.

Traction Measurement

The traction between the ball and disk was obtained by measuring the reaction force on the ball. The motor, gearbox, and loading cylinder were suspended on an air bearing which was pivoted on one end and restrained by beryllium springs on the other end. The reaction force on the ball was directly proportional to the deflection of the beryllium springs. The deflection of the springs, which was kept within 0 to 0.025 centimeter (0 to 0.010 in.), was measured with a capacitance transducer and displayed on a four-pen recorder.

Film Thickness Measurement

The EHD film thickness was measured by optical interferometry. Fringes of very good visibility were obtained by using a 17-percent-reflecting layer of chromium on the bearing surface of the transparent disks. Interference measurements were made with wavelengths of two colors (red and green). These were obtained by using a special filter and a xenon flash lamp as a light source. The details of this system and its calibration are described more fully in references 3 and 13.

Film thickness measurements under starved conditions were taken from high-speed photomicrographs by using high-speed, 35-millimeter color film. The traction and disk speed corresponding to the photomicrograph were marked by one of four pens on the four-pen recorder from a synchronized pulse of the xenon flash power supply. Typical photomicrographs with varying degrees of starvation are shown in figure 8.

Test Lubricant

The traction and starvation tests were performed with a synthetic paraffinic oil that was designated by the manufacturer as XRM 109F4. It is synthesized by the polymerization of a relatively pure mono-olefin, so it can be considered a single chemical species composed of molecules of a chain-length distribution that depends on the degree of polymerization. Some of its properties are listed in table II. The variation of viscosity with temperature, pressure, and shear stress is reported in reference 14. This fluid has also been examined in disk machines for film thickness (ref. 15) and traction (ref. 16);

and it has been tested in various full-scale bearing tests (refs. 17 to 20).

Test Conditions

Starvation and traction measurements were performed under three nominal test conditions each with a different set of material combinations to obtain three different maximum Hertzian pressures: 0.496×10^9, 1.21×10^9, and 1.90×10^9 N/m^2 (72 000, 175 000, and 275 000 psi). The corresponding material combinations were, respectively, quartz/steel ($E' = 1.1\times10^{11}$ N/m^2 (15.9×10^6 psi)), sapphire/steel ($E' = 3.29\times10^{11}$ N/m^2 (47.7×10^6 psi)), and sapphire/tungsten carbide ($E' = 6.38\times10^{11}$ N/m^2 (92.5×10^6 psi)). Although the maximum Hertzian pressures for each test varied a great deal, the material combinations provided similar elastic deformations. The elastic deformation, as represented by the Hertzian radius of contact a, is shown in table III along with the flooded film thickness $(h_0)_f$ and other test parameters. The Hertzian radius and flooded film thickness remained nearly constant for each test pressure. Thus, the departure from the Hertzian condition for each test pressure was approximately the same.

Each test was performed with the flooded film thickness corresponding to a particular interference fringe (third red fringe). The film thickness valves given in table III vary slightly for each test because the refractive index of the test fluid increases with pressure. There are eight fringes below the third red fringe from which measurements could be made when the film was starved. The two-color interferometric system allows easy interpolation between fringes.

Test Procedure

Prior to each test the bearing components shown in figure 6 were cleaned with Freon. The parts were assembled and the lubricant reservoir was filled with the test fluid. The ball was loaded against the transparent disk and driven at the speed that would establish the third red fringe in the center of the Hertzian region. The rotational velocities of the ball and disk were then recorded. In order to maintain a constant rolling velocity ($\bar{u} = 1/2(u_1 + u_2)$) during a traction run, a plot of ball velocity against disk velocity for a constant rolling speed $\bar{u}$ was then made.

A constant brake force from the hysteresis brake was then applied to the disk, and the ball velocity was adjusted to maintain a constant $\bar{u}$. A four-pen recorder recorded the traction force, disk speed, and temperature. The temperature was that of the test chamber, which was measured with a Chromel-constantan thermocouple. All tests were performed at room temperature.

The ball and disk velocities under fully flooded inlet conditions were recorded for each brake torque applied to the disk. The brake torque was increased incrementally until 100 percent sliding (zero disk velocity) was achieved.

Starved inlet conditions were obtained by gradually depleting the lubricant supply in the reservoir and on the transparent disk. Under starved inlet conditions a high-speed photomicrograph was taken for each brake force applied. The film thickness and the location of the inlet miniscus were determined from the photomicrographs.

EFFECT OF STARVATION ON FILM THICKNESS FOR ROLLING AND SLIDING

The influence of starvation on film thickness for rolling and sliding conditions is considered here. Film thickness measurements made under both rolling and sliding conditions allow a critical examination of several theoretical inlet boundary conditions.

Inlet Boundary Condition

Evaluation of pressure from the Reynolds equation requires knowledge of two boundary conditions when the side-leakage term is neglected. These are usually taken at the beginning and end of the pressure curve. For convenience, the inlet boundary condition is usually taken as $p = 0$ at $x = -\infty$. Lauder (ref. 21) has questioned this boundary condition on the grounds that it does not conform to experimental facts. Instead, he put forward the boundary condition that $p = 0$ where the fluid velocity and velocity gradient are zero (i.e., $u = \partial u/\partial z = 0$). Furthermore, it has been suggested (ref. 22) that this inlet condition could usefully be called the "oil starvation" condition, where any greater quantity of oil would result in an accumulation of oil at the inlet and any less would result in a decrease in film thickness. In addition, Capone, DeRosa, and Migliaccio (ref. 23) have used this inlet boundary condition to analyze the load capacity of rigid cylinders. Tipei (ref. 24) has analyzed inlet flow conditions by using potential flow theory and has proposed that the pressure commences at the center of two bounded vortices that develop in the inlet region.

It can be shown that these boundary conditions occur at particular locations within the inlet region. For example, $u = \partial u/\partial z = 0$ at $h/h_0 = 3$, and the Tipei boundary condition occurs at $h/h_0 = 9$. However, it can also be shown that the introduction of sliding causes these inlet boundary conditions to move downstream. For pure sliding, $u = \partial u/\partial z = 0$ at $h/h_0 = 1.5$ and the Tipei boundary condition moves downstream to $h/h_0 = 3$. It is for this reason that the theoretical load capacity of disks has been found to depend not only on the sum of the surface speeds, but also on their ratio (ref. 23). If

these fluid velocity conditions correctly describe the commencement of pressure generation (and hence the onset of starvation), we would then expect the onset of starvation to occur further downstream as the degree of sliding increases.

The starvation measurements under rolling and sliding conditions do not show this to be true. These measurements are shown in figure 9. Here the dimensionless film thickness $h_0/(h_0)_f$ is plotted aginst the starvation parameter S/S_f for all test measurements. The starvation parameter that was developed in (ref. 3) is defined as

$$\frac{S}{S_f} = \frac{Sa^{1/3}}{3.52\left[R(h_0)_f\right]^{2/3}} \tag{9}$$

where S is the inlet distance defined in figure 10, a is the Hertzian radius of contact, R is the reduced radius of curvature, and $(h_0)_f$ is the central film thickness under flooded inlet conditions. The value of h_b/h_0 corresponding to S/S_f is also given in figure 9. The experimental data given in figure 9 were obtained for various amounts of sliding, ranging from 100 percent to within a few percent of pure rolling. The experimental data show that the onset of starvation occurs approximately at an inlet location where $h_b/h_0 = 9$ and where $S/S_f = 1$. There is no indication that the onset, as well as the form of starvation, is any different under sliding conditions than it is under the rolling conditions that were described previously (ref. 3). Thus, while the Tipei boundary condition appears to describe the onset of starvation for pure rolling, it is not unique for both rolling and sliding conditions.

Inlet Flow Conditions

In order to investigate further the applicability of these fluid flow criteria to the onset of starvation, the inlet fluid flow was calculated for the experimental conditions given in figure 11.

The fluid velocity distribution within the inlet region is governed by the motion of the bearing surfaces, which attempt to transport the fluid toward the Hertzian region, and by the hydrodynamic pressure generation, which attempts to transport the fluid away from the Hertzian region. The velocity and velocity gradient can be found from (e.g. ref. 10, p. 53)

$$u = \frac{1}{2\mu}\frac{\partial p}{\partial x} z(z - h) + (u_2 - u_1)\frac{z}{h} + u_2 \tag{10}$$

$$\frac{\partial u}{\partial z} = \frac{1}{\mu}\frac{\partial p}{\partial x}\left(z - \frac{h}{2}\right) + \left(\frac{u_1 - u_2}{h}\right) \tag{11}$$

The assumptions inherent in these equations are in common with those of the Reynolds equation.

In order to avoid the complication of side leakage, the inlet flow was considered to be within an elemental strip dy along the centerline in the direction of the rolling velocity. Calculation of the velocity distribution described in equations (10) and (11) requires that the pressure gradient $\partial p/\partial x$ be known at all points within the inlet region. The pressure gradient was determined from the pressure distribution, which was calculated from the measured film shape in the following way: The measured film thickness along the centerline in the direction of motion was taken from figure 11. The measured film shape was corrected for the variation of refractive index with pressure from an estimated pressure distribution. The resulting film shape is shown in figure 12.

The general features of the corresponding pressure distribution were first deduced from the following considerations:

(1) The film thickness is very nearly constant over the center of the Hertzian region. Therefore, the pressure over this region must be very similar to the Hertzian pressure for static conditions.

(2) The termination of the pressure profile is clearly defined by the location of film rupture in the exit region, as shown in figure 11 (where it is assumed that $p = dp/dx = 0$).

(3) The location within the inlet region where pressure commences was determined from the experimental data on starvation. This is the location, under the given operating conditions, at which the film thickness becomes sensitive to the location of the inlet lubricant boundary.

(4) It can be shown that the deformation at the leading edge of the Hertzian region is greater than the corresponding Hertzian deformation for static conditions. This difference is due to the hydrodynamic pressure generated in the inlet region. This pressure must blend in with the Hertzian pressure to establish a parallel film in the Hertzian region.

(5) Near the trailing edge of the Hertzian region, the film thickness drops very suddenly into a constriction. This implies a very large pressure gradient. Furthermore, the relaxation of the surfaces into a constriction must mean that the pressure in this region is very low, much lower than the corresponding Hertzian pressure. Despite the low pressure at the rear constriction, the film thickness remains nearly constant in the region just upstream of the constriction. In fact, the interference fringes indicate a slight increase in film thickness in this region. In order to maintain this nearly parallel film, the pressure just upstream of the rear constriction must be greater than its corresponding Hertzian pressure. It is this pressure that comprises the characteristic

pressure peak under elastohydrodynamic conditions.

An initial pressure distribution was drawn in light of these considerations. Surface displacements were then computed for a line load on a semi-infinite flat solid by using the differences between the preceding pressure distribution and the Hertzian pressure distribution. The computed elastic displacements were then added to the Hertzian shape, thus giving a theoretical shape that could be compared with the measured shape. The computer program was adapted from one used by Klemz (ref. 25) for line contact. The method of calculating the surface displacements is described in (ref. 12). It was assumed that the pressure distribution in the center of the Hertzian region is Hertzian. Thus, the procedure consisted of modifying only the inlet and exit portions of the pressure curve to make the theoretical and experimental film shapes match. The inlet film shape was found to be far easier to match than the outlet film shape, where the pressure gradients are very large. The resulting pressure distribution near the exit region is, therefore, not expected to be very accurate. However, this should not significantly affect the inlet pressure distribution, which is considered here.

Having obtained a reasonable pressure distribution and film shape, as shown in figure 12, the velocity distribution at various locations within the inlet region was computed from equation (10) for pure rolling conditions ($u_1 = u_2$). For pure rolling the velocity gradient $\partial u/\partial z$ according to equation (11) equals zero at midfilm, where $z = h/2$.

The local pressure gradient and film thickness were obtained from figure 12, and the variation of viscosity with pressure was accounted for by the exponential relation of equation (3). The velocity distribution at three locations x of -2.54×10^{-4}, -2.82×10^{-4}, and -3.05×10^{-4} meter (-1.0×10^{-4}, -1.112×10^{-4}, and -1.2×10^{-4} in.) is shown in figure 13. At $x = -2.54\times10^{-4}$ meter (-1.0×10^{-4} in.) the fluid velocity distribution is very nearly equal to the surface velocity. At $x = -2.82\times10^{-4}$ meter (-1.112×10^{-4} in.) the midfilm velocity is equal to zero. This is the location of the inlet boundary condition proposed by Lauder (ref. 21), where $p = 0$ at $h/h_0 = 3$ and $u = \partial u/\partial z = 0$ at midfilm. The pressure at this location is not zero but about 3.2×10^7 N/m^2 (4700 psi). Upstream of this point some of the fluid begins to flow backward relative to the Hertzian region, as shown by the velocity distribution at $x = -3.05\times10^{-4}$ meter (-1.2×10^{-4} in.). The location of observable starvation occurs at $x = -4.01\times10^{-4}$ meter (-1.58×10^{-4} in.) (or $h/h_0 = 9$). This point, which is considerably upstream of the location where $u = \partial u/\partial z = 0$, indicates that backflow occurs over a portion of the inlet pressure buildup. Backflow is essential for the establishment of a flooded condition. Thus, the zero velocity boundary condition does not appear to provide a very good criterion for starvation. There is no physical reason why the pressure should be zero when the velocity and velocity gradient are zero. The adverse pressure gradient can cause the midfilm velocity to become negative as well as zero.

The state of affairs in the inlet region becomes apparent if we consider the volume

of lubricant required in the inlet region to obtain a flooded condition, along with the volume rate of flow. For the preceding example the required volume in the inlet region along the elemental width dy on the centerline in the direction of rolling is 134×10^{-5} dy cubic centimeter (8.2×10^{-5} dy in.^{3}), and the volume rate of flow ($q = \bar{u}h_0$ dy) is 8.2×10^{-5} dy cubic centimeter per second (0.5×10^{-5} dy in.^{3}/sec). The time required for this volume to pass through the Hertzian region, neglecting side leakage, is 16.4 seconds. The transit time for the fluid adjacent to the surfaces to travel from the inlet boundary to the exit region is only 0.0091 second. Thus, while the fluid adjacent to the surfaces is moving rapidly toward the Hertzian region, the central core of the fluid in the inlet region must remain relatively fixed (Hartung (ref. 26)). According to Tipei (ref. 24) this core forms a swirl, which appears just upstream of the point where negative velocities occur. For pure rolling, this swirl develops into two bounded vortices, which may look like that found in figure 14. The flow distribution, which is not drawn to scale, is actually very flat as the inlet distance S is typically greater than 500 h_0 when flooded. Tipei suggests that the center of the two vortices is the upstream limit of the fluid film where the Reynolds equation applies and that this location defines the condition where p = 0. Using potential flow theory, Tipei derives the following expression for the pressure gradient at the location of the vortex centers and under pure rolling conditions:

$$\frac{dp}{dx} = \frac{32}{3}\frac{\mu\bar{u}}{h^2} \tag{12}$$

Substituting in the Reynolds equation (eq. (2))

$$\frac{32}{3}\frac{\mu\bar{u}}{h^2} = 12\bar{u}\mu\left(\frac{h - h_0}{h^3}\right) \tag{13}$$

gives

$$\frac{h}{h_0} = 9 \tag{14}$$

Although this boundary condition appears to predict the onset of starvation, it is not totally unique for both sliding and rolling conditions. For pure sliding, only one vortex, which can be shown to occur at $h/h_0 = 3$, develops in the inlet region. The experimental data of figure 9, however, indicate that the onset of starvation occurs near $h/h_0 = 9$ for both rolling and sliding conditions.

The Reynolds equation implies that equivalent pressure distributions will be generated for sliding or rolling, provided the sum of the surface velocities are the same. And it has been established experimentally (refs. 27 and 28) that sliding has little effect on

film thickness. The starvation results presented in figure 9 suggest that film thickness, whether starved or flooded, is associated with the pressure generated in the inlet region. Therefore, if sliding does not alter the pressure distribution or film thickness, the location of the onset of starvation should be the same for sliding and rolling. It appears, therefore, that the inlet geometry (expressed as h/h_0) is significant, in connection with starvation, because of the pressure or pressure gradient associated with it rather than because of the particular fluid velocity distribution associated with it. The fluid velocity distribution may be more important in connection with how the fluid is transported into the inlet region. It has been observed experimentally that starvation tends to be much more severe when the condition of 100 percent sliding is reached.

EFFECT OF STARVATION ON TRACTION

The influence of starvation on traction is now considered. The traction force for each of the three test conditions is plotted against the slide-roll ratio in figures 15 to 17. The slide-roll ratio is defined as

$$\text{Slide-roll ratio} = \frac{u_1 - u_2}{\frac{1}{2}(u_1 + u_2)} \tag{15}$$

The denominator is the average velocity of the fluid passing through the Hertzian region and is by definition equal to the rolling velocity $\bar{u}$. The numerator is the sliding velocity between the ball and the disk. At 100 percent sliding ($u_2 = 0$) the value of the slide-roll ratio as defined in equation (15) is 2.

The solid lines in figures 15 to 17 show how the traction varies with the slide-roll ratio under flooded conditions. There are three general features of the traction curves under flooded conditions:

(1) The traction force rises to a maximum as the slide-roll ratio increases. No well-defined traction peaks were observed.

(2) The traction force rises to a maximum more rapidly as the maximum Hertzian pressure increases.

(3) The maximum traction coefficients increase with the Hertzian pressure. For the three test pressures (0.496×10^9, 1.21×10^9, and 1.90×10^9 N/m^2; 72 000, 175 000, and 275 000 psi) the maximum traction coefficients (defined as traction force divided by normal load) are respectively 0.038, 0.055, and 0.065.

The open circles in figures 15 to 17 are the measured tractions observed under various degrees of starvation. The significant feature of the results is that in all cases tested a starved film was observed to possess greater traction than a flooded film for the

same slide-roll ratio. Also, it was observed that operation under 100-percent sliding ($u_2 = 0$) always resulted in a greater degree of starvation than when $u_2 > 0$. Thus, the measured traction was found to be relatively higher for 100 percent sliding.

In reference 3 the influence of starvation on film thickness has been successfully analyzed by normalizing film thickness and the location of the inlet boundary by using their corresponding values under flooded conditions. Hence, we obtained the dimensionless film thickness parameter $h_0/(h_0)_f$ and the dimensionless inlet boundary parameters S/S_f and h_b/h_0. These parameters generalize the starved elastohydrodynamic problem for other conditions of operation. The influence of starvation on traction is more difficult to analyze in this way. The reasons are the same as those that make it more difficult to predict traction than film thickness under flooded conditions. Except at very low sliding speeds the problem can no longer be considered isothermal, and the rheological behavior of the fluid becomes complicated and ill defined.

In order to analyze the general effect of starvation on traction, it was assumed that the elastic deformation is Hertzian (i.e., a parallel film of thickness h_0) and that the traction is dominated by the shear conditions in the Hertzian region for a Newtonian fluid.

For isothermal conditions and $\alpha p >> 1$, the traction force can be estimated by (ref. 29)

$$T = \frac{2\pi a^2 \mu_0 e^{\alpha p}}{\alpha p} \times \frac{(u_1 - u_2)}{h_0} \tag{16}$$

A starved film simply increases the shear rate $(u_1 - u_2)/h_0$ since h_0 decreases when starved. If isothermal conditions prevailed, the traction would be inversely proportional to h_0. This is the assumption made by Archard and Baglin (ref. 30), who present a dimensionless analysis of traction under starved conditions. This assumption leads to the condition that the increase in traction due to starvation is the inverse of the decrease in film thickness due to starvation. Thus, we can write

$$\frac{T}{T_f} = \left[\frac{h_0}{(h_0)_f}\right]^{-1} \tag{17}$$

where the subscript f refers to a flooded condition. Because the film thickness reduction is a known function of the starvation parameter S/S_f, we then have

$$\frac{T}{T_f} = \left[\frac{h_0}{(h_0)_f}\right]^{-1} = f\left(\frac{S}{S_f}\right) \tag{18}$$

Since the prevailing conditions are not isothermal, the effect of starvation on heat generation and heat conduction must be considered. In reference 31 the heat generation q_v is given as

$$q_v = \mu_0 e^{\alpha p} \left(\frac{u_1 - u_2}{h_0} \right)^2 \tag{19}$$

where it is seen that the heat generation is proportional to the square of the shear rate $(u_1 - u_2)/h_0$. For a constant sliding velocity a starved film will increase the heat generation.

The temperature of the oil film in the Hertzian region depends on the ability of the surfaces to conduct the heat away. It is shown in reference 31 that the major factor affecting the thermal condition of the system is the ratio of the time of transit through the Hertzian region to the time constant associated with the thermal conduction of the surfaces. This is represented by the dimensionless parameter

$$\Lambda = \frac{kt_0}{h_0^2} \tag{20}$$

where k is the thermal conductivity of the fluid and t_0 is the time of transit through one-half of the Hertzian region ($t_0 = a/\bar{u}$). For our experiments, t_0 is constant since $\bar{u}$ was kept constant for all sliding conditions. A starved film increases Λ by way of its smaller values of h_0. The essence of a thinner film is that it improves the heat transfer to the bearing surfaces.

Figure 18 shows the increase in traction T/T_f as a function of the starvation parameter S/S_f. The solid curve in figure 18 represents the theory as proposed by Archard and Baglin (ref. 30) which assumes that the increase in traction due to starvation is the inverse of the decrease in film thickness due to starvation. Because of thermal and perhaps some rheological effects the theory provides a convenient upper bound to the data.

The preceding equations show that the shear rate $(u_1 - u_2)/h_0$ and film thickness h_0 play an important role in traction for a Newtonian fluid. For this reason the traction results are considered in terms of shear rate. Figure 19 shows the measured traction force as a function of shear rate for all the test conditions. The solid curves represent the traction under flooded conditions. The flooded curves have the same shape as those in figures 15 to 17. Under flooded conditions the shear rate reaches a limiting value at 100 percent sliding. There are two general features of the starved results in figure 19:

(1) A starved film can produce much higher shear rates than a flooded one. For example, measured shear rates were found to increase an order of magnitude, from

40×10^4 seconds^{-1} to 400×10^4 seconds^{-1}, when the film became severely starved.

(2) Except for very low shear rates, traction under a starved condition is greater than traction under a flooded condition. This is expected if we consider the thermal conditions of equations (19) and (20). At a constant shear rate the heat generation, according to equation (19), will be the same for all degrees of starvation. The heat conduction, however, improves as the film becomes thinner by starvation. This should lower the film temperature and, therefore, increase the traction.

The traction behavior was quite different when the shear rates were low. This is shown in figures 20 to 22, where the region of low shear rate for each test condition has been expanded. The solid curves again represent traction under flooded conditions. The dashed curves show traction under various degrees of starvation. The unexpected feature of the results is that as the shear rate became smaller and the oil film in the Hertzian region became more starved, the measured traction force became very much lower than the flooded value.

These results do not appear to be explainable in terms of a Newtonian fluid subjected to viscous heating. A tentative explanation may be arrived at by considering the effect of starvation on the shear conditions in the inlet region and the recent evidence of Adams and Hirst (ref. 32), who have associated the high shear stresses in the inlet region with non-Newtonian behavior in this region.

Figure 8 shows that as starvation becomes more severe the film shape tends toward the Hertzian shape. The pressure distribution, therefore, must also tend toward the Hertzian pressure distribution. Thus, as the inlet boundary approaches the leading edge of the Hertzian region, the inlet pressure gradient will become more severe. This has been shown by the full computer solution of Castle and Dowson (ref. 6) for the starved film thickness problem in line contact. Thus, very high shear stresses must be associated with the severe pressure gradient developed in the inlet region under severely starved conditions.

The results appear to suggest that at high shear rates the traction is dominated by the shear conditions in the Hertzian region. When the shear rates are low in the Herzian region, the influence of the rheological behavior of the fluid in the inlet region begins to appear. This rheological behavior is associated with the severe shear conditions developed by the large pressure gradients generated in the inlet region under starved conditions.

It can be argued that if traction under starved conditions is influenced by rheological behavior in the inlet region, film thickness must also be influenced by the same rheological behavior. Although the film thickness data of figure 9 appear to be somewhat lower than theory would predict for severely starved conditions, it must be noted that the measurement of the location of the inlet boundary S becomes very difficult under severely starved conditions, as shown in figure 8(c). The experimental error in the data of fig-

ure 9 is too great to make any comment on the effect of rheological behavior on film thickness under severely starved conditions.

EFFECT OF PRESSURE ON FILM THICKNESS

An additional experiment was performed to determine the influence of pressure on film thickness since it is shown in reference 15 that the influence of pressure on film thickness is much greater than theory predicts. The effect of pressure on film thickness is shown in figure 23. Here the central film thickness h_0 and the film thickness at the rear h_r and side h_s constrictions are plotted as a function of the maximum Hertzian pressure. These measurements were performed with the sapphire/steel material combination and the same lubricant used in the traction measurements. The absolute value of the central film thickness h_0, as well as its variation with pressure, agrees with the film thickness theory of reference 3. That theory is also plotted in figure 23. The sensitive effect of pressure on film thickness was not observed here as it was in reference 15 for line contact under much higher rolling velocities. The film thickness at the side constrictions h_s was more sensitive to pressure than h_0 or h_r. This effect has been observed elsewhere (ref. 33).

SUMMARY OF RESULTS

Traction and film thickness have been measured under starved elastohydrodynamic conditions for a nominal point-contact geometry. Measurements were obtained for three maximum Hertzian pressures: 0.496×10^9, 1.21×10^9, and 1.90×10^9 N/m^2 (72 000, 175 000, and 275 000 psi). Optical interferometry was used to measure film thickness. The major results are summarized as follows:

1. The presence of sliding does not affect the manner in which the film thickness varies with the location of the inlet boundary under starved conditions.

2. The location of certain fluid velocity conditions suggested in the literature, such as zero velocity and velocity gradient and the centers of vortices that develop in the inlet region, do not adequately define the commencement of pressure generation and the onset of starvation. The experimental measurements and theory show that a dimensionless gap thickness of 9 in the inlet region adequately defines the onset of starvation for both rolling and sliding conditions. With this inlet boundary condition, it is shown by using a Reynolds lubrication analysis that backflow occurs over a portion of the inlet region where hydrodynamic pressure is generated.

3. In all cases tested a starved film was observed to possess greater traction than a flooded film for the same slide-roll ratio.

4. For a constant slide-roll ratio the maximum shear rate in the Hertzian region increased with the degree of starvation. Measured shear rates are defined as $(u_1 - u_2)/h_0$, where u_1 and u_2 are the surface velocity of ball and disk, respectively, and h_0 is the film thickness at the center of the Hertzian region. Measured shear rates were found to increase an order of magnitude from 40×10^4 seconds^{-1} to 400×10^4 seconds^{-1} when the film becomes severely starved.

5. Because of the importance of thermal effects, the traction measurements were considered in terms of the shear rate $(u_1 - u_2)/h_0$ within the Hertzian region. In this way the flooded and starved traction measurements could be compared under similar conditions of heat generation. Except for low rates of shear, the measured traction under starved conditions was found to be greater than the traction under flooded conditions for the same shear rate. This can be explained in terms of improved heat conduction when the film is starved.

6. When the shear rates in the Hertzian region were low and the film was severely starved, the measured values of traction were found to be much lower than expected. It is tentatively suggested that this may be explained in terms of the high shear stresses developed by the large pressure gradient that occurs within the inlet region when it is severely starved. Thus, the shear history of the fluid in the inlet region may affect the traction developed in the Hertzian region.

7. Measurement of central film thickness under flooded conditions to a maximum Hertzian pressure of 1.90×10^9 N/m^2 (275 000 psi) showed good agreement with theory.

Lewis Research Center,
National Aeronautics and Space Administration,
Cleveland, Ohio, July 25, 1975,
505-04.

REFERENCES

1. Signer, H.; Bamberger, E. N.; and Zaretsky, E. V.: Parametric Study of the Lubrication of Thrust Loaded 120-mm Bore Ball Bearings to 3 Million DN. J. Lubr. Tech., Trans. ASME, Ser. F, vol. 96, no. 3, July 1974, pp. 515-524.

2. DeWinter, A.; and Blok, H.: Fling-Off Cooling of Gear Teeth. ASME Trans., J. Engr. Industry, vol. 96, no. 1, Feb. 1974, pp. 60-70.

3. Wedeven, L. D.; Evans, D.; and Cameron, A.: Optical Analysis of Ball Bearing Starvation. J. Lubr. Tech., Trans. ASME, Ser. F, vol. 93, no. 3, July 1971, pp. 349-363.

4. Orcutt, F. A.; and Cheng, H. S.: Lubrication of Rolling-Contact Instrument Bearings. Proc. Gyro Spin-Axis Hydrodynamic Bearing Sym., vol. 2, chapt. 5, Massachusetts Inst. of Tech., 1966, Tab. 5, pp. 1-25.

5. Wolveridge, P. E.; Baglin, K. P.; and Archard, J. G.: Starved Lubrication of Cylinders in Line Contact. Proc. Instr. Mech. Engrs., vol. 185, 1971, pp. 1159-1171.

6. Castle, P.; and Dawson, D.: A Theoretical Analysis of the Starved Elastohydrodynamic Lubrication Problem for Cylinders in Line Contact. Elastrohydrodynamic Lubrication Sym., Inst. of Mech. Engrs., 1972, pp. 131-137.

7. Wymer, D.: Discussion of Ref. 6, Elastrohydrodynamic Lubrication Sym., Inst. of Mech. Engrs., 1972, p. 197.

8. Dalmaz, G.; and Godet, M.: An Apparatus for the Simultaneous Measurement of Load, Traction and Film Thickness in Lubricated Sliding Point Contacts. Tribology. vol. 5, no. 3, June 1972, pp. 111-117.

9. Smith, R. L.; Walowit, J. A.; and McGrew, J. M.: Elastohydrodynamic Traction Characteristics of 5P4E Polyphenyl Ether. J. Lubr. Tech., Trans. ASME, Ser. F, vol. 95, no. 3, July 1973, pp. 353-362.

10. Cameron, Alastair: Principles of Lubrication. John Wiley & Sons, Inc., 1966.

11. Barus, C.: Isothermals, Isopiestics and Isometrics Relative to Viscosity. Amer. J. Sci., vol. 45, 1893, pp. 87-96.

12. Dowson, D.; and Higginson, G. R.: Elastohydrodynamic Lubrication, The Fundamentals of Roller and Gear Lubrication. Pergamon Press, Ltd., 1966.

13. Foord, C. A.; Wedeven, L. D.; Westlake, F. J.; and Cameron, A.: Optical Elastohydrodynamics. Proc. Inst. Mech. Engrs., vol. 184, pt. 1, 1969-1970, pp. 487-505.

14. Carlson, S.; Turchina, V.; Jakobsen, J.; Sanborn, D. M.; and Winer, W. O.: Investigation of Lubricant Rheology as Applied to Elastohydrodynamic Lubrication. (Georgia Inst. of Tech.; Grant NGR-11-002-133.) NASA CR-134539, 1973.

15. Parker, Richard J.; and Kannel, Jerold W.: Elastohydrodynamic Film Thickness Between Rolling Disks with a Synthetic Paraffinic Oil to 589 K (600° F). NASA TN D-6411, 1971.

16. Trachman, Edward G.; and Cheng, H. S.: Rheological Effects on Friction in Elastohydrodynamic Lubrication. NASA CR-2206, 1973.

17. Rhoads, W. L.; and Peacock, L. A.: Advanced Turbine Engine Mainshaft Lubrication System Investigation, Phase 2. Part 1: Background, Test Elements and

Results, and Conclusions for System Performance. (SKF-AL69T016, SKF Industries, Inc.; NAS3-6267.) NASA CR-72854, 1971.

18. Loomis, William R.; Townsend, Dennis P.; and Johnson, Robert L.: Lubricants for Inerted Lubrication Systems in Engines for Advanced Aircraft. SAE Paper 680317, Apr.-May 1968.

19. Rhoads, W. L.; and Sibley, L. B.: Supersonic Transport Lubrication System Investigation, Phase 1. (SKF-AL67T060, SKF Industries, Inc.; NAS3-6267.) NASA CR-54662, 1967.

20. Chiu, Y. P.; Hahn, D.; and Rosenberg, N.: Exploratory Analysis of Elastohydrodynamic Properties of Lubricants. SKF-AL72P001, SKF Industries, Inc. (AD-739390; QPR-2), 1971.

21. Lauder, W.: Hydrodynamic Lubrication of Proximate Cylindrical Surfaces of Large Relative Curvature. Proc. Inst. of Mech. Engrs., vol. 180, pt. 3B, 1965-66, pp. 101-106.

22. Whitaker, A. V.: Communication. Proc. Inst. Mech. Engrs., vol. 180, pt. 3B, 1965-66, p. 246.

23. Capone, E.; DeRosa, E.; and Migliaccio, M.: A Study of the Lubrication of Discs. Wear, vol. 22, 1972, pp. 91-103.

24. Tipei, N.: Boundary Conditions of a Viscous Flow Between Surfaces with Rolling and Sliding Motion. ASME Trans., Ser. F., vol. 90, no. 1, Jan. 1968, pp. 254-261.

25. Klemz, B.: Stress Measured by Photoelasticity. Ph. D. Thesis, University of London, 1970.

26. Hartung, H. A.: Entrance Space in Rolling Contacts. ASME Paper 65-WA/LUB-5, Nov. 1965.

27. Crook, A. W.: The Lubrication of Rollers. II - Film Thickness with Relation to Viscosity and Speed. Phil. Trans. Roy. Soc. (London), Ser. A, vol. 254, 1961-62, pp. 223-236.

28. Dyson, A.; Naylor, H.; and Wilson, A. R.: The Measurement of the Oil-Film Thickness in Elastohydrodynamic Contacts. Proc. Inst. Mech. Engrs., vol. 180, pt. 3B, 1965-66, pp. 119-134.

29. Gu, A.; and Walowit, J.: Discussion. J. Lubr. Tech., ASME Trans., Ser. F., vol. 93, no. 3, July 1971, pp. 346-347.

30. Archard, J. F.; and Baglin, K. P.: Nondimensional Presentation of Frictional Tractions in Elastohydrodynamic Lubrication. II - Starved Conditions. J. Lubr. Tech., Trans. ASME, Ser. F, vol. 97, no. 3, July 1975, pp. 412-423.

31. Wolveridge, P. E.; and Archard, J. F.: Temperature Distribution in Elastohydrodynamic Films, A New Analytic Solution. Elastrohydrodynamic Lubrication Sym., Inst. of Mech. Engrs., 1972, pp. 48-54.

32. Adams, D. R.; and Hirst, W.: Frictional Traction in Elastohydrodynamic Lubrication. Proc. Roy. Soc. (London), Ser. A, vol. 332, 1973, pp. 505-525.

33. Foord, C. A.; Hammann, W. C.; and Cameron, A.: Evaluation of Lubricants Using Optical Elastohydrodynamics. ASLE Trans., vol. 11, no. 1, Jan. 1968, pp. 31-43.

TABLE I. - MECHANICAL PROPERTIES OF TEST MATERIALS

Material	Compressive strength		Modulus of elasticity		Poisson's ratio	Specific heat		Thermal conductivity at 293 K (20° C)	
	N/m^2	psi	N/m^2	psi		J/(kg)(K)	Btu/(lb)(°F)	W/(m)(K)	cal/(sec)(cm)(°C)
Quartz	1.14×10^9	166×10^3	70.3×10^9	10.2×10^6	0.17	840	0.20	1.4	0.0033
Sapphire	2.07	300	465.0	67.5	.47	750	.18	38	.092
Steel	1.38	200	207.0	30.0	.30	500	.12	50	.12
Tungsten carbide	5.18	752	641.0	93.0	.25	130	.03	17	.041

TABLE II. - PROPERTIES OF SYNTHETIC PARAFFINIC OIL

Viscosity, m^2/sec (cS):	
At 17.8° C (0° F)	0.037 (37 000)
At 37.8° C (100° F)	0.000447 (447)
At 98.9° C (210° F)	0.0000404 (40.4)
At 149° C (300° F)	0.000013 (13)
At 204° C (400° F)	0.000006 (6)
Density, g/cm^3:	
At 37.8° C (100° F)	0.8389
At 93.3° C (200° F)	0.8082
At 149° C (300° F)	0.7777
At 204° C (400° F)	0.7428
Pressure-viscosity coefficient,[a] α, $(N/m^2)^{-1}$ $((psi)^{-1})$:	
At 37.8° C (100° F)	1.99×10^{-8} (1.37×10^{-4})
At 99° C (210° F)	1.51×10^{-8} (1.04×10^{-4})
At 149° C (300° F)	1.29×10^{-8} (0.89×10^{-4})
Refractive index at 26° C (78.8° F)	1.4689
Flash point, °C (°F)	271 (520)
Fire point, °C (°F)	313 (595)
Pour point, °C (°F)	-51 (-60)
Specific heat, J/(kg)(K) (Btu/(lb)(°F))	
At 149° C (300° F)	2.66×10^3 (0.635)
At 204° C (400° F)	2.90×10^3 (0.692)
Surface tension, N/cm (dyne/cm)	30.3×10^{-5} (30.3)

[a]From ref. 14; defined as $(\alpha)^{-1} = \int_0^\infty \mu_0 \, dp/\mu(p)$.

TABLE III. - TEST CONDITIONS

	Test condition		
	1	2	3
Maximum Hertzian pressure, p_{max}, N/m^2 (psi)	0.496×10^9 (72 000)	1.21×10^9 (175 000)	1.90×10^9 (275 000)
Load, N (lbf)	22.3 (5)	37.8 (8.5)	36.7 (8.25)
Hertzian radius, a, m (in.)	0.149×10^{-3} (5.87×10^{-3})	0.121×10^{-3} (4.77×10^{-3})	0.096×10^{-3} (3.79×10^{-3})
Material combination	Quartz/steel	Sapphire/steel	Sapphire/tungsten carbide
Rolling velocity, $\bar{u} = \frac{1}{2}(u_1 + u_2)$, m/sec (in./sec)	0.1366 (5.38)	0.1540 (6.06)	0.1554 (6.12)
Test temperature, ^{o}C (^{o}F)	23.5 (74.3)	24 (75.2)	24 (75.2)
Inlet distance necessary to obtain flooded film thickness, $S_f = \frac{3.52\left[R(h_0)_f\right]^{2/3}}{a^{1/3}}$, m (in.)	0.222×10^{-3} (8.74×10^{-3})	0.23×10^{-3} (9.06×10^{-3}	0.241×10^{-3} (9.49×10^{-3})
Flooded film thickness, $(h_0)_f$, μm (μin.)	0.592 (23.3)	0.562 (22.1)	0.538 (21.2)

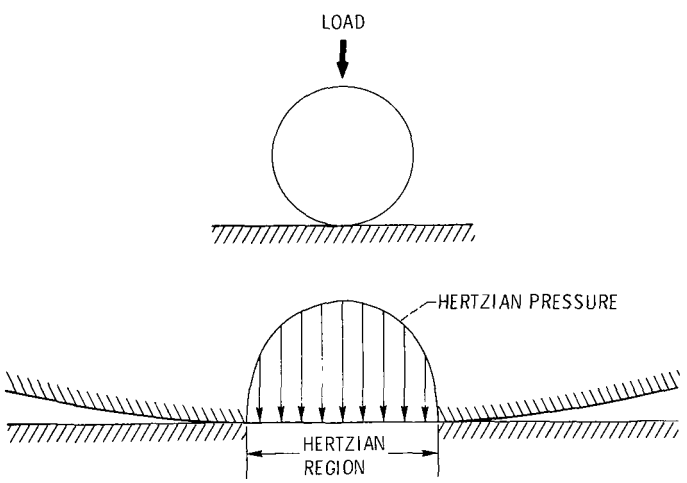

Figure 1. - Hertzian condition of static contact.

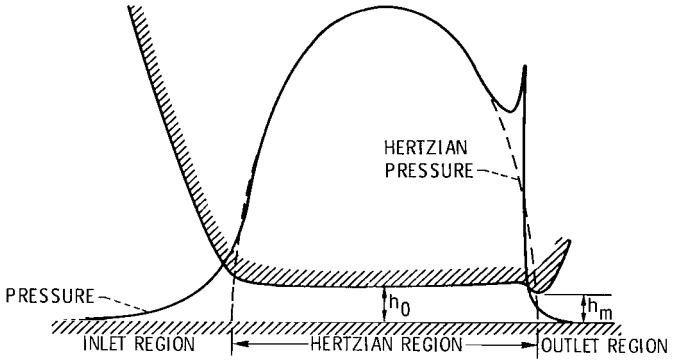

Figure 2. - Three general regions of elastohydrodynamic conjunction.

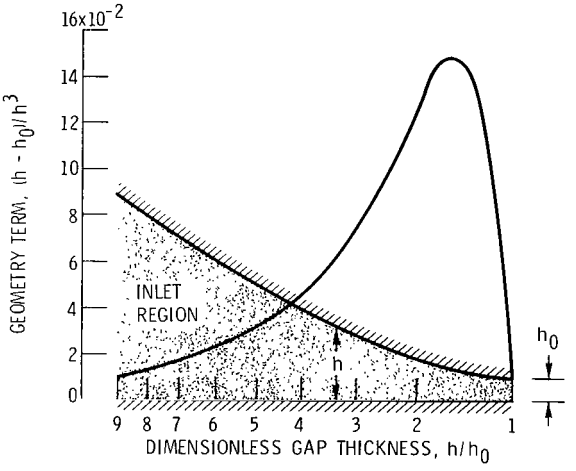

Figure 3. - Geometry term as function of dimensionless gap thickness.

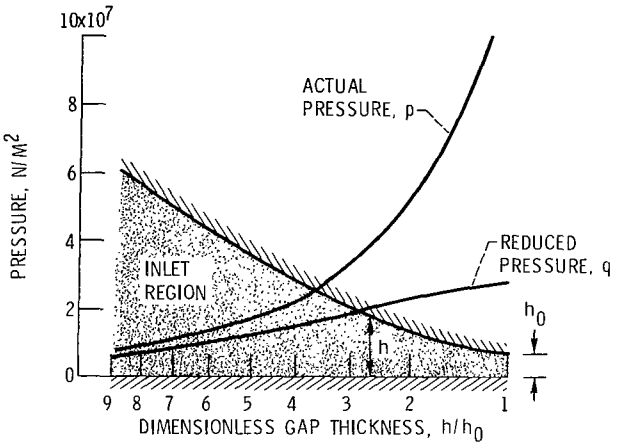

Figure 4. - Actual pressure and reduced pressure as function of dimensionless gap thickness.

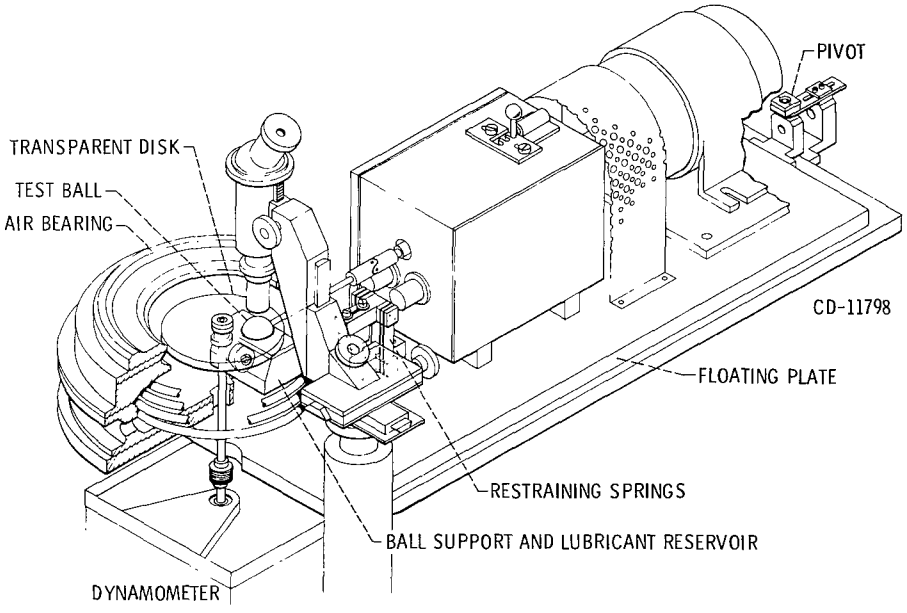

Figure 5. - Optical elastohydrodynamic apparatus.

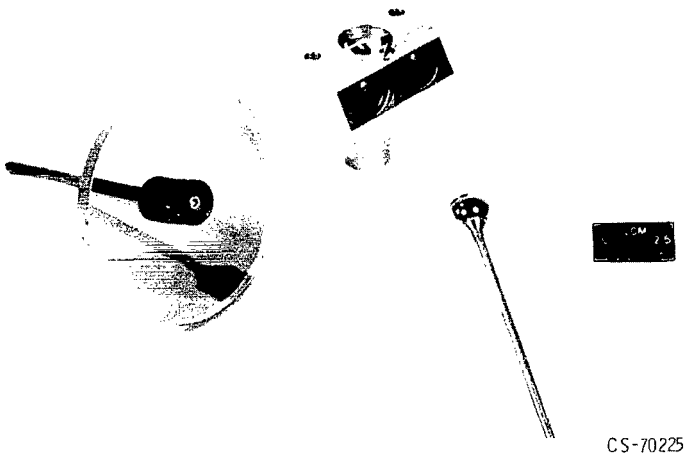

Figure 6. - Test ball, transparent disk, and lubricant reservoir.

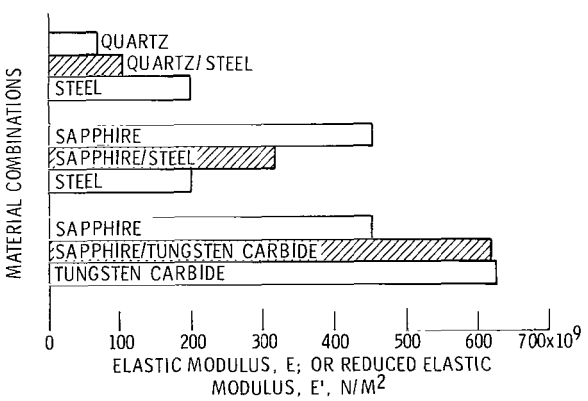

Figure 7. - Elastic modulus and reduced elastic modulus for test materials.

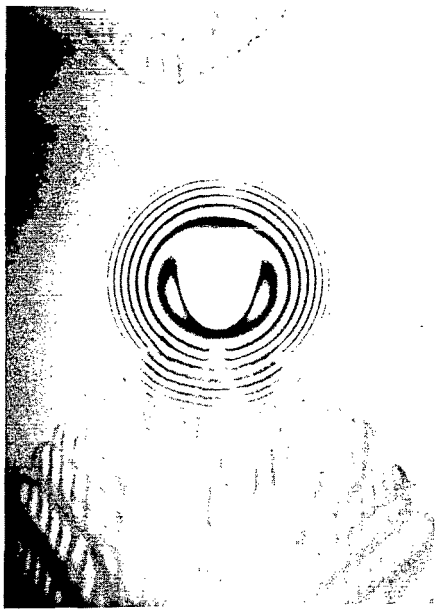

(a) $S = 25.9X10^{-3}$ cm ($10.2X10^{-3}$ in.); $h_0 = 0.50$ μm (20 μin.); $\bar{u} = 15.5$ cm/sec (6.10 in./sec); $u_1 - u_2 = 15.6X10^{-2}$ cm/sec (0.0614 in./sec); traction force, 1.0 N (0.10 lbf).

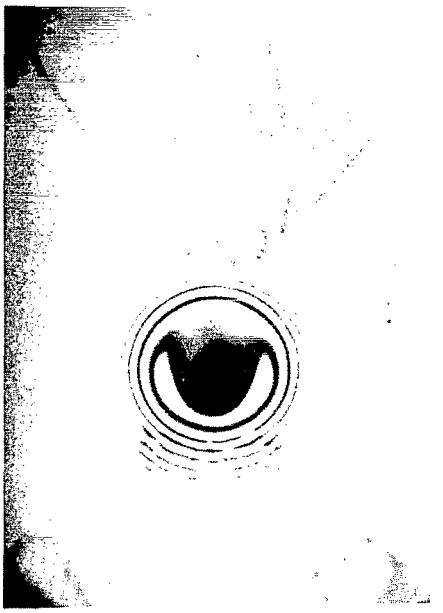

(b) $S = 9.1X10^{-3}$ cm ($3.58X10^{-3}$ in.); $h_0 = 0.370$ μm (14.6 μin.); $\bar{u} = 15.3$ m/sec (6.02 in./sec); $u_1 - u_2 = 72.2X10^{-2}$ cm/sec (0.284 in./sec); traction force, 1.84 N (0.188 lbf).

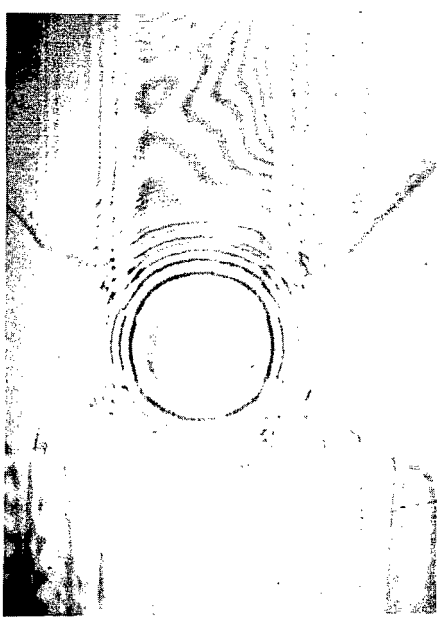

(c) $S = 2.3X10^{-3}$ cm ($0.91X10^{-3}$ in.); $h_0 = 0.08$ μm (3.15 μin.); $\bar{u} = 15.56$ cm/sec (6.13 in./sec); $u_1 - u_2 =$ 31.12 cm/sec (12.3 in./sec) – pure sliding; traction force, 3.22 N (0.328 lbf).

Figure 8. - Typical photomicrographs showing effect of starvation on film thickness (inlet distance measured from inlet lubricant boundary to leading edge of Hertzian region, S; film thickness at center of Hertzian region, h_0; rolling velocity, $\bar{u}$; difference in surface velocities of ball and disk, $u_1 - u_2$; and traction force). Material combination, sapphire/tungsten carbide; load, 36.7 N (8.25 lbf); maximum Hertzian pressure, p_{max}, $1.90X10^9$ N/m^2 (275 000 psi); central film thickness under flooded conditions, $(h_0)_f$, 0.538 μm (21.2 μin.).

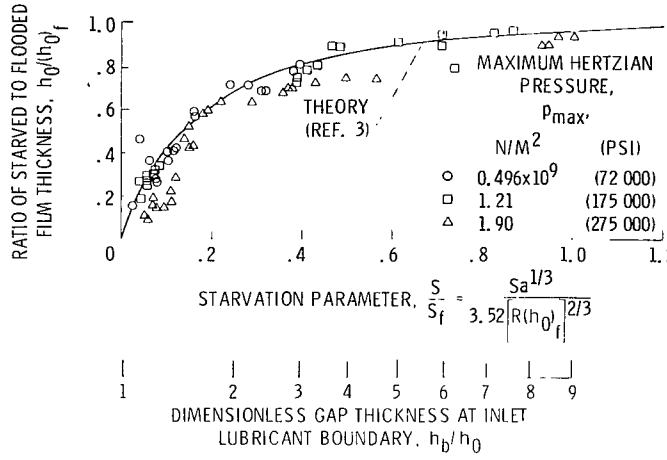

Figure 9. - Variation of film thickness with starvation for rolling and sliding conditions.

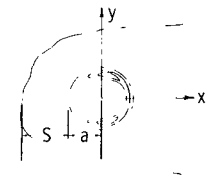

(a) Plan view.

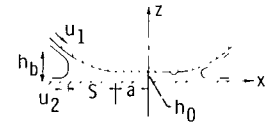

(b) Cross-sectional view along centerline.

Figure 10. - Contact geometry showing required measurements for starvation.

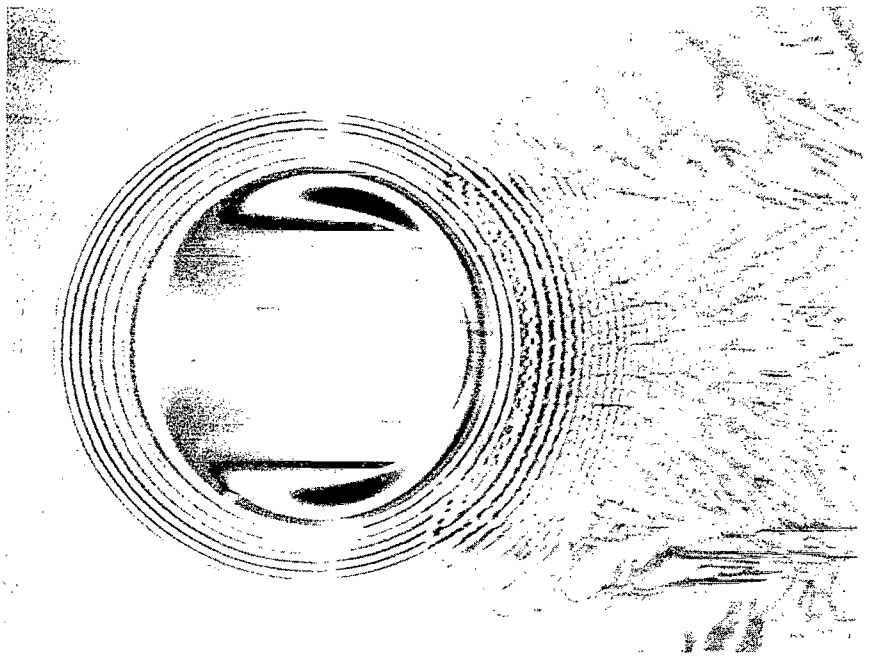

Figure 11. - Photomicrograph of optical interference fringes formed between a steel ball and a glass surface. Reduced radius of contact, R, 1.27 cm (0.5 in.); load 53 N (5.4 lbf); maximum Hertzian pressure, p_{max}, 0.6×10^9 N/m^2 (87 000 psi); reduced elastic modulus, E', 1.17×10^{11} N/m^2 (17×10^6 psi); rolling velocity, $\bar{u}$, 6.96 cm/sec (2.74 in./sec); ambient viscosity of lubricant, μ_0, 2.63×10^{-5} N-sec/m^2 (54.9×10^{-6} lbf-sec/ft^2); pressure-viscosity coefficient, α, 3.67×10^{-8} (N/m^2)$^{-1}$ (2.5×10^{-4} (psi)$^{-1}$).

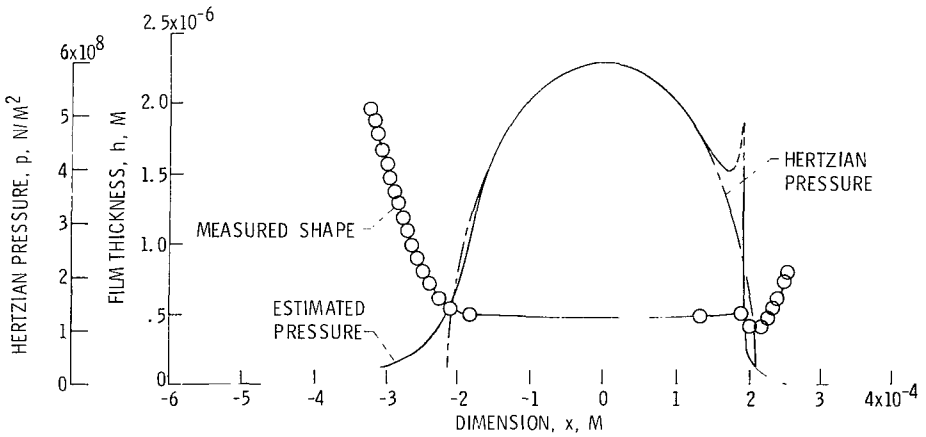

Figure 12. - Measured film shape and estimated pressure distribution along centerline in direction of rolling.

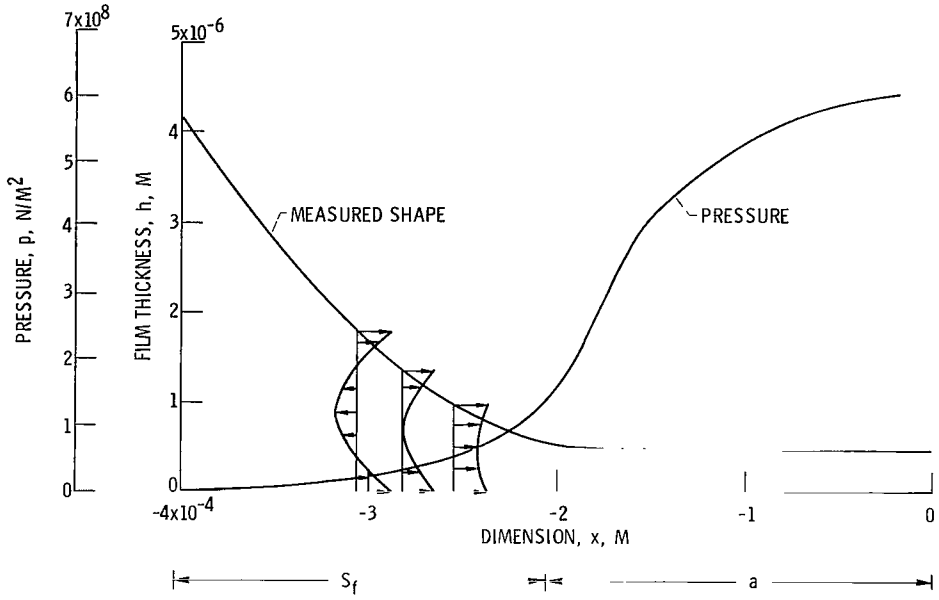

Figure 13. - Fluid velocity distributions at different locations within inlet region.

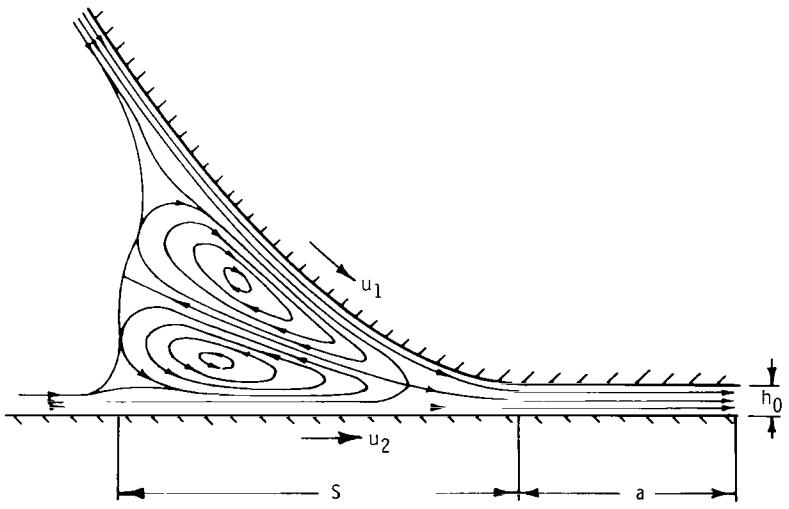

Figure 14. - Flow distribution within convergent inlet region.

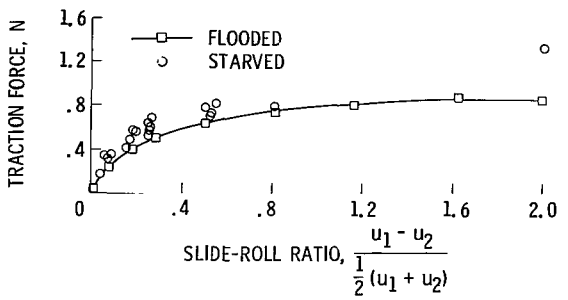

Figure 15. - Variation of traction with slide-roll ratio under starved and flooded conditions for test condition 1: maximum Hertzian pressure, p_{max}, 0.496×10^9 N/m^2 (72 000 psi); material combination, quartz/steel; Hertzian radius, a, 0.149×10^{-3} m (5.87×10^{-3} in.); load, 22.3 N (5 lbf).

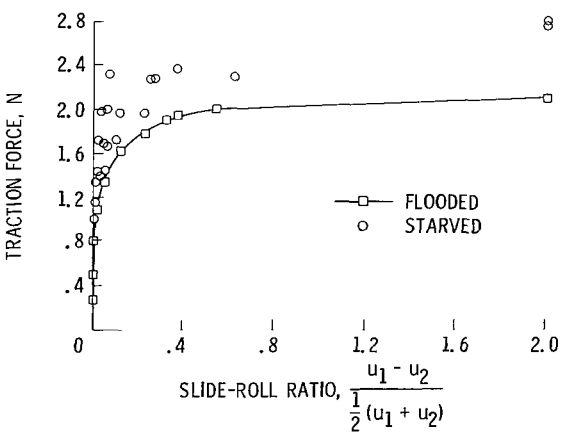

Figure 16. - Variation of traction with slide-roll ratio under starved and flooded conditions for test condition 2: maximum Hertzian pressure, p_{max}, 1.21×10^9 N/m^2 (175 000 psi); material combination, sapphire/steel; Hertzian radius, a, 0.121×10^{-3} m (4.77×10^{-3} in.); load, 37.8 N (8.5 lbf).

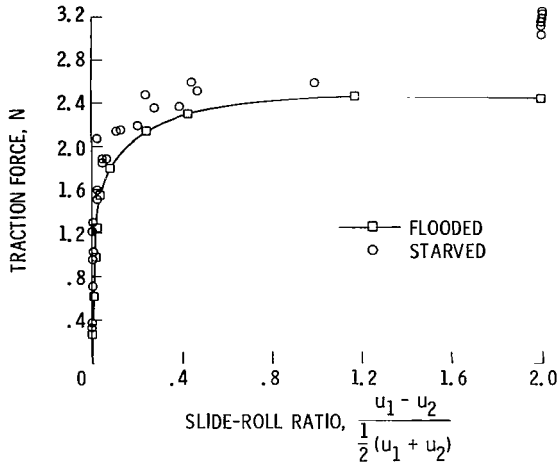

Figure 17. - Variation of traction with slide-roll ratio under starved and flooded conditions for test condition 3; maximum Hertzian pressure, p_{max}, 1.90×10^9 N/m^2 (275 000 psi); material combination, sapphire/tungsten carbide; Hertzian radius, a, 0.096×10^{-3} m (3.79×10^{-3} in.); load, 36.7 N (8.25 lbf).

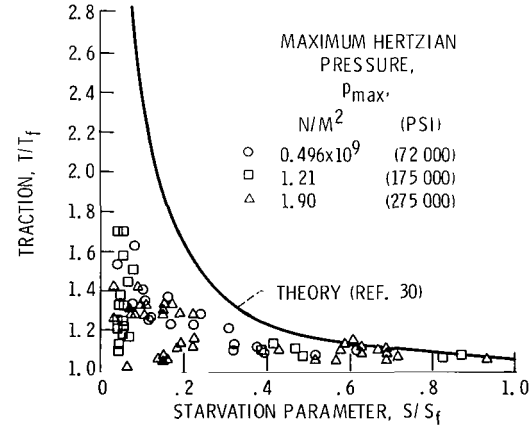

Figure 18. - Influence of starvation on traction.

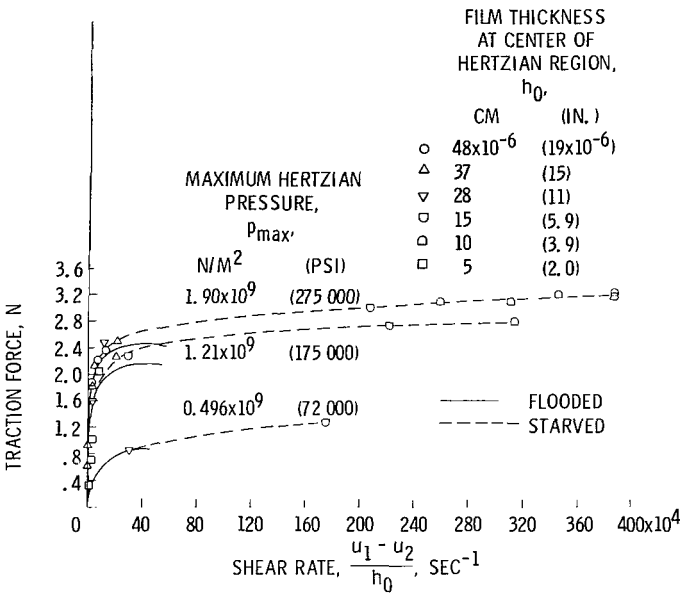

Figure 19. - Variation of traction with shear rate and maximum Hertzian pressure under starved and flood conditions.

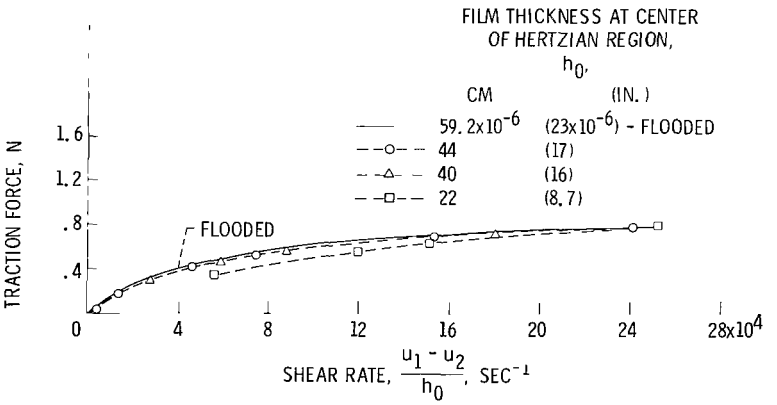

Figure 20. - Variation of traction with shear rate under starved and flooded conditions for test condition 1: maximum Hertzian pressure, p_{max}, 0.496x10^9 N/m^2 (72 000 psi); material combination, quartz/steel; Hertzian radius, a, 0.149x10^{-3} m (5.87x10^{-3} in.); load, 22.3 N (5 lbf).

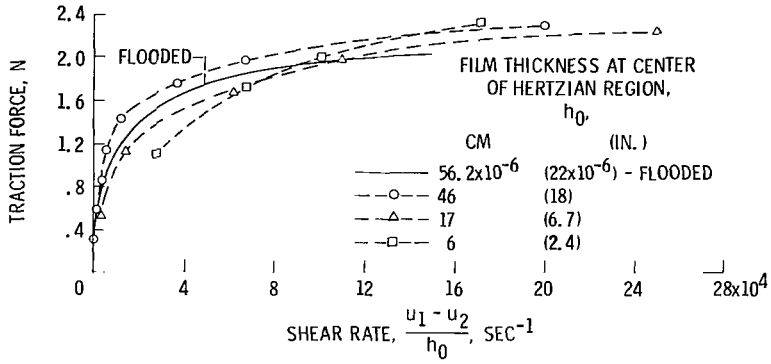

Figure 21. - Variation of traction with shear rate under starved and flooded conditions for test condition 2: maximum Hertzian pressure, p_{max}, 1.21×10^9 N/m^2 (175 000 psi); material combination, sapphire/steel; Hertzian radius, a, 0.121×10^{-3} m (4.77×10^{-3} in.); load, 37.8 N (8.5 lbf).

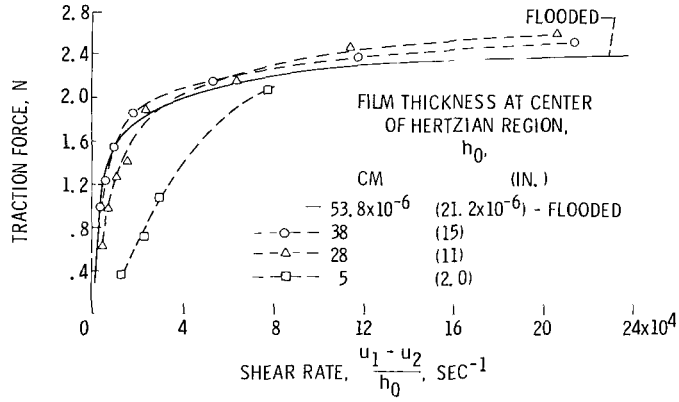

Figure 22. - Variation of traction with shear rate under starved and flooded conditions for test condition 3: maximum Hertzian pressure, p_{max}, 1.90×10^9 N/m^2 (275 000 psi); material combination, sapphire/tungsten carbide; Hertzian radius, a, 0.096×10^{-3} m (3.79×10^{-3} in.); load, 36.7 N (8.25 lbf).

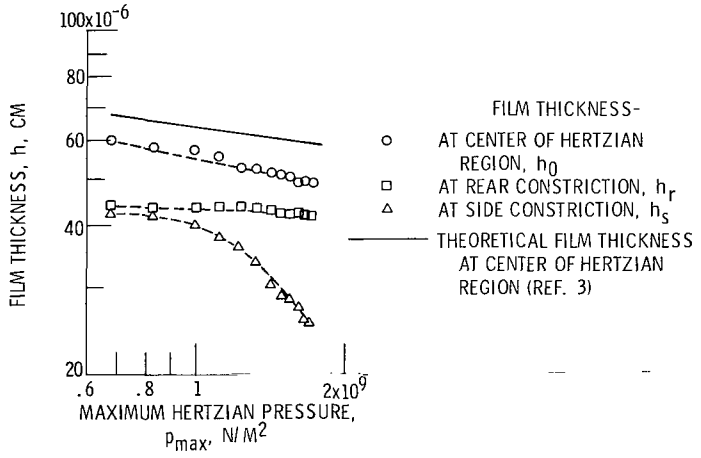

Figure 23. - Variation of film thickness with maximum Hertzian pressure. Material combination, sapphire/steel; rolling velocity, $\bar{u}$, 17.05 cm/sec (6.71 in./sec).